First published in:

Available online at www.sciencedirect.com

SCIENCE DIRECT®

Computational Materials Science 37 (2006) 306–317

COMPUTATIONAL MATERIALS SCIENCE

www.elsevier.com/locate/commatsci

Studies on rate-dependent switching effects of piezoelectric materials using a finite element model

Arunachalakasi Arockiarajan [a], Buelent Delibas [a], Andreas Menzel [a,*], Wolfgang Seemann [b]

[a] *Chair of Applied Mechanics, University of Kaiserslautern, P.O. Box 3049, D-67653 Kaiserslautern, Germany*
[b] *Institute of Engineering Mechanics, University of Karlsruhe, Kaiserstr. 12, D-76131 Karlsruhe, Germany*

Received 31 May 2005; received in revised form 2 August 2005; accepted 22 August 2005

Abstract

The main goal of this paper consists in the modeling of rate-dependent behavior of piezoelectric materials within a three-dimensional finite element setting. We propose a rate-dependent polarization framework which is applied to cyclic electrical loading at various frequencies. The reduction in free energy of a grain is used as a criterion for the onset of the domain switching process. Nucleation in new grains and propagation of the domain walls during domain switching is modeled by a linear kinetics theory. Averaging over all individual grains renders the macroscopic response of the bulk material. Intergranular effects, which are essential for realistic simulations, are phenomenologically captured via a probabilistic approach. The presented numerical examples, as based on the proposed three-dimensional finite element framework, are related to the simulation of PIC-151 ceramics. In particular, averaged electric displacement versus electric field curves are plotted and compared with experimental data reported in the literature.

Keywords: Piezoelectric materials; Domain switching; Rate-dependent polarization; Probabilistic approach; Linear kinetics theory; Finite elements

1. Introduction

In recent years, piezoelectric and ferroelectric materials such as $BaTiO_3$, PZT, PLZT ceramics have widely been used for the design of smart materials and intelligent systems, see e.g., Jaffe et al. [20]. Under the action of low electric fields or low mechanical stresses, the behavior of these materials is almost linear but exhibits strong non-linear response under high electric fields or mechanical stresses. Polarization switching in the domains is identified as the main reason for this non-linearity which plays an important role for piezoelectric applications. Such switching processes in the underlying unit cells or rather grains involve a reorientation of the electric dipoles. The principal crystallographic directions (e.g., the *c* axis in a tetragonal cell) align according to the orientation of these dipoles which causes a change in mechanical strain. The domain switching in polycrystals is in general not homogeneous since the domain walls, which separate different phases, move through the crystal. In order to better understand and explain the non-linear properties of piezoelectric and ferroelectric materials under high electromechanical loadings, many experiments have been performed and reported in the literature; the reader is referred to the contributions by Cao and Evans [5], Hwang et al. [16], Lynch [27], Lu et al. [26] and references cited in these works. Research on the modeling of non-linear response of piezoceramics can be classified into two major approaches:

On the one hand, micromechanical models focus on individual domains as for instance discussed by Hwang et al. [16], Chen et al. [7], Fotinich and Carman [11], Huber and Fleck [14] or Elhadrouz et al. [9]. These models are commonly based on randomly oriented bulk elements whereby microcrystalline properties are assumed for the behavior of each individual element. The macroscopic behavior of these models is usually analysed by means of

* Corresponding author. Tel.: +49 631 205 2126; fax: +49 631 205 2128.
E-mail address: amenzel@rhrk.uni-kl.de (A. Menzel).
URL: http://mechanik.mv.uni-kl.de (A. Menzel).

0927-0256/$ - see front matter © 2005 Elsevier B.V. All rights reserved.
doi:10.1016/j.commatsci.2005.08.008

volume averaging techniques. Concerning the switching process, Hwang et al. [16] introduced a work energy criterion to determine the initialization of domain switching. The interaction among grains in the underlying domain has thereby been addressed by using an Eshelby inclusion method, see also Hwang et al. [15]. A finite element model at the meso-scale has been developed by Hwang and McMeeking [17,18] considering purely ferroelectric and ferroelastic poly-crystals. Hwang and Waser [19] simulated the domain switching in a poly-crystalline ferroelectric and ferroelastic ceramic using a micromechanical approach. In order to reduce the computational effort, piezoelectric effects have, however, been neglected. Another micromechanical model has been proposed by Chen et al. [7], which takes multiple domains into account and additionally incorporates the interaction between the domains by means of a mean field theory. Fotinich and Carman [11,12] developed a domain switching criterion based on a critical value of the electric displacement due to switching with additional stability arguments for mono-crystalline piezoceramics. They also addressed the influence of the orientation distribution on the material response for random—, layer— and single-domain mixtures.

On the other hand, macroscopic models have been suggested, which incorporate particular sets of state variables entering for instance a phenomenological motivated free energy function. In this context, Chen and Peercy [6] proposed a formulation where aligned dipoles are included in the constitutive relations. Based on a thermodynamically consistent setting, Zhang and Rogers [37] developed a phenomenological framework for elecromechanical coupling effects. The dielectric behavior is thereby described with the help of a hyperbolic function. Another phenomenological model for ferroelectric materials has been advocated by Kamlah and Tsakmakis [23] which is straightforwardly based on the introduction of reasonable internal variables. The constitutive behavior is governed by appropriate ordinary differential equations capturing the history dependence of the material. Kamlah and Böhle [22] proposed a finite element model based on a two step staggered scheme: firstly, the purely dielectric boundary value problem is solved for the electric potential. Secondly, the electric potential is prescribed and the electromechanical analysis for the mechanical boundary conditions finally yields the mechanical stress field. A monolithic coupled finite element formulation has recently been elaborated by Romanowski and Schröder [31,33]. That approach is essentially based on a set of appropriate evolution equations, which, conceptually speaking, incorporate a one-dimensional switching criterion, and embedded into a thermodynamically consistent framework.

In general, the macroscopic behavior of poly-crystalline ferroelectric materials is rate-dependent; the reader is referred to the contribution by Landis [25] for a survey of the thermodynamically consistent modelling of switching effects including rate-dependencies. Jiang [21] mentioned that the coercive field becomes larger with increasing frequencies (from 1 to 100 Hz) of the applied alternating electric field. The experimental response of the polarization and the strain under electric loading with different amplitudes and frequencies is analyzed in Zhou et al. [38]. These studies show that the coercive field increases with increasing loading frequency. Smith et al. [36] developed a model for rate-dependent hysteresis at low excitation frequency ranges. This formulation additionally captures the movement of domain walls. Moreover, the authors are able to show a reduction of remanent polarization for increasing frequencies—the prediction of the change in the coercive field, however, is not completely accurate. Kim and Jiang [24] developed a three-dimensional finite element model for rate-dependent behavior of ferroelectric ceramics associated with domain switching. The free energy thereby serves for the characterization of the constitutive behavior of ferroelectric variants. Propagation of polarization switching after its onset is modeled in terms of continuous changes of mass fractions and a kinetic relation. Numerical simulations underline the expansion of the hysteresis curve for increasing loading frequencies.

The aim of the present work is to develop a three-dimensional finite element model for the rate-dependent behavior of piezoelectric materials including domain switching. A large number of crystallites with randomly distributed polarization orientations are taken into account whereby each crystallite corresponds to one finite element. The onset of the domain switching is not only determined in terms of the free energy but also by a probabilistic model. As the key feature of this approach, switching occurs with a certain probability which depends on the fraction of free energy with respect to a critical energy level, see Seemann et al. [34]. The dependence of the probability on this ratio can be modeled in terms of analytical functions, e.g., by polynomials or hyperbolic functions. With this probabilistic approach in hand, intergranular effects are phenomenologically taken into account. Rate-dependent behavior, however, takes the interpretation as the wall, which separates the two phases before and after switching, propagating through the domain with a certain velocity. This effect is captured by a linear kinetics relation so that nucleation starts in a particular grain after the switching process has been initiated. Simulations are carried out under electrical loading with various frequencies and amplitudes which linearly increase and decrease in time. The results of this model are compared with measured hysteresis loops given in the literature by means of plotting the electric displacement versus the electric field.

The paper is organized as follows: Section 2 reviews some aspects of fundamental balance— and constitutive relations of ferroelectric and ferroelastic materials. The reader is referred to the monographs by Nye [30], Eringen [10] or Greiner [13] and references cited in these works for detailed background information. The proposed rate-dependent model is discussed in Section 3 while we briefly review the corresponding finite element setting in Section 4. For further details concerning the numerical framework as

well as implementational aspects see, e.g., Schröder and Gross [32] and the monograph by Silvester and Ferrari [35]. Representative numerical examples are elaborated in Section 5 and the paper is concluded with a short summary, see Section 6.

2. Constitutive model

The lattice structure of the considered ferroelectric material possesses cubic symmetry for operating temperatures above the Curie temperature. This phase is called paraelectric whereby, practically speaking, the relative atom positions in the crystal lattice give rise to a vanishing net dipole moment. Consequently, no piezoelectric effect is observed within this phase. Depending on the particular composition of the material, however, the underlying phases possibly change if the temperature is reduced below the Curie temperature. Apparently, the symmetry of the material might switch from simple cubic structures to tetragonal or rhombohedral arrangements. The new phase is denoted as the ferroelectric phase. Relative position of atoms are modified according to this phase transformation, say, so that a non-zero net dipole moment is observed. This net polarization is commonly introduced as spontaneous polarization. It occurs in the microstructure and stems from the specific arrangement of relative positions of atoms in the ferroelectric phase. The movements of atoms during the phase transition renders an additional lattice distortion which, moreover, results in mechanical strains. This strain is usually called the spontaneous strain. In what follows, essential constitutive relations of the previously highlighted physical phenomena are reviewed.

Let B denote a body of interest with configuration $\mathscr{B} \subset \mathbb{R}^3$ determined by placements $\boldsymbol{x} \in \mathbb{R}^3$. The essential degrees of freedom are provided by the displacement field $\boldsymbol{u} \in \mathbb{R}^3$ together with the electric potential $\phi \in \mathbb{R}$. Equilibrium of B for the quasi-static case is represented via

$$\begin{aligned} \boldsymbol{0} &= \nabla \cdot \boldsymbol{\sigma} + \boldsymbol{b} && \text{in } \mathscr{B}, \\ \boldsymbol{u} &= \boldsymbol{u}^{\mathrm{p}} && \text{on } \partial\mathscr{B}_u, \\ \boldsymbol{t} &= \boldsymbol{t}^{\mathrm{p}} = \boldsymbol{\sigma} \cdot \boldsymbol{n}_\sigma && \text{on } \partial\mathscr{B}_\sigma \end{aligned} \tag{1}$$

with $\partial\mathscr{B}_u \cup \partial\mathscr{B}_\sigma = \partial\mathscr{B}, \partial\mathscr{B}_u \cap \partial\mathscr{B}_\sigma = \emptyset$ and

$$\begin{aligned} 0 &= \nabla \cdot \boldsymbol{D} && \text{in } \mathscr{B}, \\ \phi &= \phi^{\mathrm{p}} && \text{on } \partial\mathscr{B}_\phi, \\ -q &= -q^{\mathrm{p}} = \boldsymbol{D} \cdot \boldsymbol{n}_D && \text{on } \partial\mathscr{B}_D \end{aligned} \tag{2}$$

with $\partial\mathscr{B}_\phi \cup \partial\mathscr{B}_D = \partial\mathscr{B}$, $\partial\mathscr{B}_\phi \cap \partial\mathscr{B}_D = \emptyset$. Following standard notations, the stress tensor and the electric displacement field have thereby been denoted as $\boldsymbol{\sigma} = \boldsymbol{\sigma}^{\mathrm{t}} \in \mathbb{R}^{3\times3}$ and $\boldsymbol{D} \in \mathbb{R}^3$ and $\boldsymbol{n}_{\sigma,D} \in \mathbb{R}^3$ characterize unit normals to the corresponding surfaces.

Classical linear constitutive equations of a piezoelectric material in the piezoelectric phase are given by

$$\boldsymbol{\sigma} = \mathbf{C} : \boldsymbol{\varepsilon} - \boldsymbol{E} \cdot \boldsymbol{d}, \tag{3}$$

$$\boldsymbol{D} = \boldsymbol{d} : \boldsymbol{\varepsilon} + \boldsymbol{\epsilon} \cdot \boldsymbol{E}, \tag{4}$$

where $\boldsymbol{\varepsilon} = \boldsymbol{\varepsilon}^{\mathrm{t}} = \nabla^{\mathrm{sym}}\boldsymbol{u} \in \mathbb{R}^{3\times3}$ denotes the strain tensor while $\boldsymbol{E} = -\nabla\phi \in \mathbb{R}^3$ represents the electric field. Material parameters are incorporated via $\mathbf{C} = \mathbf{C}^{\mathrm{t}} = \mathbf{C}^{\mathrm{T}} \in \mathbb{R}^{3\times3\times3\times3}$, $\boldsymbol{\epsilon} = \boldsymbol{\epsilon}^{\mathrm{t}} \in \mathbb{R}^{3\times3}$ and $\boldsymbol{d} \in \mathbb{R}^{3\times3\times3}$ which are introduced as the elastic stiffness, the dielectric permittivity and the piezoelectric tensor, respectively.

The so-called non-linear constitutive equations of the piezoelectric material additionally incorporate a spontaneous polarization vector and a spontaneous strain tensor. The extension of Eqs. (3) and (4) consequently renders

$$\boldsymbol{\sigma} = \mathbf{C} : [\boldsymbol{\varepsilon} - \boldsymbol{\varepsilon}^{\mathrm{s}}] - \boldsymbol{E} \cdot \boldsymbol{d}, \tag{5}$$

$$\boldsymbol{D} = \boldsymbol{d} : [\boldsymbol{\varepsilon} - \boldsymbol{\varepsilon}^{\mathrm{s}}] + \boldsymbol{\epsilon} \cdot \boldsymbol{E} + \boldsymbol{P}^{\mathrm{s}}, \tag{6}$$

wherein $\boldsymbol{P}^{\mathrm{s}} \in \mathbb{R}^3$ and $\boldsymbol{\varepsilon}^{\mathrm{s}} = [\boldsymbol{\varepsilon}^{\mathrm{s}}]^{\mathrm{t}} \in \mathbb{R}^{3\times3}$, with $\mathrm{tr}(\boldsymbol{\varepsilon}^{\mathrm{s}}) = 0$, characterize the spontaneous polarization and spontaneous strain, respectively. For poly-crystalline materials at virgin—i.e. electrically un-poled—state, the polarization vector field is in general randomly oriented. Practically speaking, each grain is divided into sub-domains of different polarization orientation. Since the direction of the polarization is equally distributed in the virgin state, the polarization of the bulk material vanishes at the macro level. If the material is sufficiently loaded with respect to, e.g., a prescribed electric field, the polarization vectors within the grains align according to this loading direction. A graphical representation of these effects is shown in Fig. 1.

Even though material parameters generally change during switching processes, the elastic stiffness and the dielectric permittivity are commonly assumed to remain constant. Moreover, anisotropic response in mainly caused by the piezoelectric constant which supports the assumptions

$$\mathbf{C} = \lambda \boldsymbol{I} \otimes \boldsymbol{I} + 2\mu \mathsf{I}^{\mathrm{sym}}, \tag{7}$$

$$\boldsymbol{\epsilon} = \epsilon \boldsymbol{I}, \tag{8}$$

wherein λ and μ are the Lamé parameters, ϵ essentially characterizes the dielectric permittivity and $\boldsymbol{I}$ and I denote identity tensors of second and fourth order. The piezoelectric constant, however, captures the modeling of anisotropic behavior. We are in particular interested in piezoelectric materials of perovskite type with tetragonal

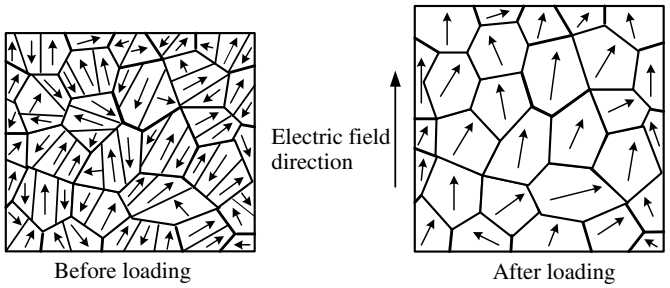

Fig. 1. Two-dimensional illustration of domains with underlying grains of a poly-crystalline piezoelectric material: un-poled virgin state (left) and poled state after electrical loading (right).

microstructure. The directions which characterize this symmetry group, 4 mm, are denoted by unit vectors $\boldsymbol{m}$. Apparently, the six possible orientation of $\boldsymbol{m}$ are in the $\langle 100\rangle$ family. In view of the piezoelectric constant we consequently introduce

$$\boldsymbol{d} = d_{33}\boldsymbol{M} + d_{31}[\boldsymbol{m}\otimes\boldsymbol{I} - \boldsymbol{M}] + d_{15}\left[\frac{1}{2}[\boldsymbol{I}\otimes\boldsymbol{m} + \boldsymbol{I}\overline{\otimes}\boldsymbol{m}] - \boldsymbol{M}\right], \tag{9}$$

wherein $\boldsymbol{M} = \boldsymbol{m}\otimes\boldsymbol{m}\otimes\boldsymbol{m}$ and $[\boldsymbol{I}\otimes\boldsymbol{m} + \boldsymbol{I}\overline{\otimes}\boldsymbol{m}] : \boldsymbol{a} = [\boldsymbol{I}\otimes\boldsymbol{m} + \boldsymbol{I}\overline{\otimes}\boldsymbol{m}] : \boldsymbol{a}^{\mathrm{t}}\ \forall \boldsymbol{a}\in\mathbb{R}^{3\times3}$. The main reason for non-linear behavior of the material stems from domain switching effects in the microstructure. Due to the fact that the polarization vector is aligned with $\boldsymbol{m}$, which are in the $\langle 100\rangle$ family, solely two types of domain switching come into the picture, namely 90° and 180° domain switching. The particular angle denotes the rotation of the polarization vector so that, for a given polarization, four different formats of 90° switching are possible while only one meaningful 180° switching occurs. A crystallite microstructure is commonly considered to switch, if the reduction of free energy ΔU exceeds a particular energy barrier. In this work we adopt the switching criterion, along with boundary conditions, advocated by McMeeking and Hwang [28]. To be specific, it is assumed that

$$\Delta U(\boldsymbol{u},\phi) + V_{\mathrm{c}}\Delta\psi_{\mathrm{c}} \leqslant 0, \tag{10}$$

whereby $\Delta\psi_{\mathrm{c}}$ denotes a constant energy barrier per unit volume and V_{c} represents the volume of the crystallite which switches. If switching occurs, the spontaneous polarization $\boldsymbol{P}^{\mathrm{s}}$ of the crystallite is assumed to change solely its direction at constant amount $P^{\mathrm{s}} = \|\boldsymbol{P}^{\mathrm{s}}\|$ of the polarization vector, i.e.,

$$\begin{aligned} &\boldsymbol{P}^{\mathrm{s}}_{n+1} = \boldsymbol{P}^{\mathrm{s}}_{n} + \Delta\boldsymbol{P}^{\mathrm{s}} \quad \text{with} \\ &\Delta\boldsymbol{P}^{\mathrm{s}} = P^{\mathrm{s}}[\boldsymbol{m}_{n+1} - \boldsymbol{m}_{n}]. \end{aligned} \tag{11}$$

The indices $n+1$ and n thereby refer to the underlying time interval $\Delta t = t_{n+1} - t_n > 0$. For notational simplicity, however, the index $n+1$ is often also omitted.

Similarly, the spontaneous strain of the crystallite might switch as well. By analogy with the polarization vector, we assume $\varepsilon^{\mathrm{s}} = \|\boldsymbol{\varepsilon}^{\mathrm{s}}\|$ to remain constant and require $\mathrm{tr}(\boldsymbol{\varepsilon}^{\mathrm{s}}) = 0$ which results in

$$\begin{aligned} &\boldsymbol{\varepsilon}^{\mathrm{s}}_{n+1} = \boldsymbol{\varepsilon}^{\mathrm{s}}_{n} + \Delta\boldsymbol{\varepsilon}^{\mathrm{s}} \quad \text{with} \\ &\Delta\boldsymbol{\varepsilon}^{\mathrm{s}} = \frac{3}{2}\varepsilon^{\mathrm{s}}[\boldsymbol{m}_{n+1}\otimes\boldsymbol{m}_{n+1} - \boldsymbol{m}_{n}\otimes\boldsymbol{m}_{n}]. \end{aligned} \tag{12}$$

As previously mentioned, it is assumed that the dielectric constant and the elastic modulus are unaffected by the switching. In what follows, we adopt the change of energy in the system to be approximated by means of the ansatz

$$\Delta U = \boldsymbol{E}\cdot\Delta\boldsymbol{P}^{\mathrm{s}} + \boldsymbol{\sigma} : \Delta\boldsymbol{\varepsilon}^{\mathrm{s}} \tag{13}$$

as advocated in Hwang et al. [16]. This relation will be incorporated into the switching criterion in Eq. (10) which enables us to compute representative numerical examples in the progression of this work.

Apparently, the constitutive framework reviewed so far fits into the class of coupled problems. The degrees of freedom, namely $\boldsymbol{u}$ and ϕ, are coupled via the balance relations (1) and (2) and the constitutive Eqs. (5) and (6). Please note that any change in spontaneous polarization or spontaneous strain consequently contributes to the iterative calculation of the displacement field and the electric potential, respectively.

3. Rate-dependent model

The dependence of the electric field and the temperature on the switching time and the switching current has been investigated in Merz [29] by means of experiments for $BaTiO_3$ single-crystals. A reduction in switching time, and consequently an increase of the switching current, has been noticed for increasing temperatures at constant electric field in that study. The observed switching mechanism thereby stems from the nucleation of new domains. Subsequently, growth processes due to domain wall motions take place. At higher temperatures both, the nucleation of domains and the growth processes, develop faster than at lower temperatures. Abeyarate et al. [1] developed a model based on the free energy function, a kinetic relation and a nucleation criterion. The switching response of each individual phase was thereby described by means of a constitutive theory. Subsequently, the nucleation criterion signals the phase transition which is characterized by a kinetic relation based on thermal activation theory. Arlt [3,2,4] proposed a model within which the propagation of the new phase is dominated by the phase boundary between the old and the new nucleated phases. Particular kinetic relations are proposed in order to determine the growth of the new phase. For quasi-static loading, which is assumed in these contributions, domain switching must be completed within each individual load increment. In other words, if the incremental load step takes place in a rather short time interval, domain switching might not be finished. Considering for instance cyclic loading experiments, different electric displacement versus electric field curves can be observed for different loading frequencies.

In this work we apply a linear kinetics theory for the propagation of the new phase, which has been proposed in Delibas et al. [8]. The underlying switching criterion, as introduced in Eqs. (10) and (13), is thereby evaluated at zero stresses $\boldsymbol{\sigma}$ and consequently boils down to

$$\boldsymbol{E}\cdot\Delta\boldsymbol{P}^{\mathrm{s}} > 2E_0P_0, \tag{14}$$

whereby V_{c} is supposed to remain constant. The coercive electric field parameter is denoted by $E_0 > 0$ while $P_0 > 0$ characterizes the (maximum) magnitude of the polarization vector; compare Hwang et al. [16]. As a key feature of this model, a critical time duration of the switching process is introduced whenever nucleation has been initiated. In general, this critical time parameter takes different values

for each individual incremental loading. If the time interval between two subsequent incremental steps is larger than this critical time period, the phase boundary can completely propagate through the domain, i.e., the switching process can be completed. The critical time parameter, which can also be interpreted as the minimum time required for the quasi-static case, is called the limit time Δt_{l}. Based on experimental results, Merz [29] suggested the following relation:

$$\Delta t_{\mathrm{l}} = \frac{\beta d}{E - E_0} \quad \text{with } E = \|\boldsymbol{E}\| \tag{15}$$

for the limit time, wherein β, $d > 0$ characterize a temperature-dependent material parameter and the thickness of the specimen, respectively. Eq. (15) reflects that the initiation of switching processes occurs only if the applied electric field exceeds the coercive electric field, i.e., $E - E_0 > 0$; compare Eq. (14). In practice, initiation of switching processes are observed even before the macroscopically measured coercive electric field is attained. Due to this fact, we propose the following ansatz for the limit time

$$\Delta t_{\mathrm{l}} = \frac{C}{E} \quad \text{with } C = \beta d > 0, \tag{16}$$

so that, conceptually speaking, the coercive electric field E_0 is assumed to be zero within the proposed relation for Δt_{l}. For purpose of illustration of the rate-dependent model, we consider a uniaxial setting under cyclic loading in terms of ϕ. The electric potential is thereby fixed to zero at the bottom of the specimen, ϕ_{bot}, and chosen to depend on time at the top of the specimen, ϕ_{top}; see Figs. 2 and 5 for a graphical representation. The frequency of the applied electric potential is given by

$$f_\phi = \frac{1}{T_\phi}, \tag{17}$$

wherein T_ϕ denotes the time period for a full cycle according to Fig. 2. For this particular case, the rate of change of the electric potential $\dot{\phi}_{\mathrm{top}}$ reads

$$\dot{\phi}_{\mathrm{top}} = \pm \frac{2\widehat{\phi}}{\frac{1}{2}T_\phi} = \pm 4\frac{\widehat{\phi}}{T_\phi} = \pm 4\widehat{\phi} f_\phi \tag{18}$$

with $\widehat{\phi}$ being the loading amplitude of the electric potential. The increment of electric potential $\Delta\phi_{\mathrm{top}}$ between

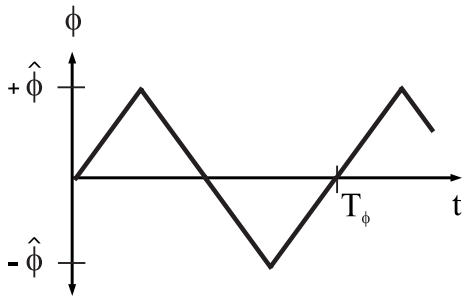

Fig. 2. Triangular cyclic loading.

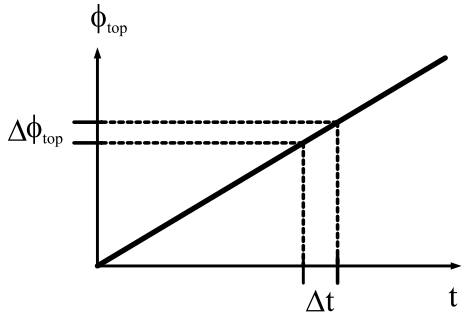

Fig. 3. Incremental loading.

two load steps is prescribed and renders essential boundary conditions. Fig. 3 shows that such a load increment corresponds to a finite time step $\Delta t = t_{n+1} - t_n > 0$, for which

$$\Delta t = \frac{\Delta\phi_{\mathrm{top}}}{\dot{\phi}_{\mathrm{top}}} = \frac{\Delta\phi_{\mathrm{top}}}{4\widehat{\phi} f_\phi} \tag{19}$$

holds. Eq. (19) underlines that the time interval Δt decreases for increasing frequencies of the electric potential. For the subsequent numerical simulations $\Delta\phi_{\mathrm{top}}$ and $\widehat{\phi}$ are assumed to remain constant. In case that the switching process is active in a particular domain but Δt turns out to be smaller than Δt_{l}, the change in polarization direction is not to be completed within the time step Δt. Based on the applied linear kinetics theory, only a fraction of the domain of interest has undergone a phase change. This volume ratio is represented by $\Delta t/\Delta t_{\mathrm{l}}$. If Δt is rather small, for instance due to a higher frequency f_ϕ, the domain switching process might take several time steps until the whole domain has switched.

Next, we elaborate the volume fraction which defines the switched domain part ΔV in relation to the total volume V. In this regard, the time period $\Delta t_{\mathrm{p}} \leqslant \Delta t_{\mathrm{l}}$ is introduced, which represents the time elapsed since the initiation of the nucleation process, namely

$$\Delta V = V\frac{\Delta t_{\mathrm{p}}}{\Delta t_{\mathrm{l}}} \quad \text{so that } \frac{\Delta V}{V} = \frac{\Delta t_{\mathrm{p}}}{\Delta t_{\mathrm{l}}}. \tag{20}$$

Please note that Δt_{p} might be a multiple of Δt. Furthermore, let $\boldsymbol{P}^{\mathrm{s}}_n$ and $\widehat{\boldsymbol{P}}^{\mathrm{s}}_{n+1}$ denote polarization vectors in the domain of interest. Switching is assumed to be initiated within the underlying time interval Δt. Moreover, the notation $\widehat{\boldsymbol{P}}^{\mathrm{s}}_{n+1}$ refers to the situation where the phase change has been completed. Based on the applied linear kinetic theory, the actual polarization vector $\boldsymbol{P}^{\mathrm{s}}_{n+1}$ allows representation as

$$\boldsymbol{P}^{\mathrm{s}}_{n+1} = \frac{\Delta V}{V}\widehat{\boldsymbol{P}}^{\mathrm{s}}_{n+1} + \left[1 - \frac{\Delta V}{V}\right]\boldsymbol{P}^{\mathrm{s}}_n \tag{21}$$

for $\Delta t_{\mathrm{l}} \geqslant \Delta t$. Replacing the volume fractions with respect to Eq. (20) results in

$$\boldsymbol{P}^{\mathrm{s}}_{n+1} = \frac{\Delta t_{\mathrm{p}}}{\Delta t_{\mathrm{l}}}\widehat{\boldsymbol{P}}^{\mathrm{s}}_{n+1} + \left[1 - \frac{\Delta t_{\mathrm{p}}}{\Delta t_{\mathrm{l}}}\right]\boldsymbol{P}^{\mathrm{s}}_n. \tag{22}$$

Since the time interval of interest is subdivided into several subintervals Δt we might relate, for instance, Δt_{p} or Δt_{l} to

Δt. In this regard, let t_s denote the time step at which switching is initiated, so that the following relation

$$\Delta t_p = -t_s + \sum_n [t_{n+1} - t_n] = \sum_{t_s}^{t_n} \Delta t \dot{\leqslant} z\Delta t \tag{23}$$

holds for $\Delta t_p \geqslant \Delta t$, wherein z is some positive integer. Nucleation after one time step consequently results in

$$\boldsymbol{P}^s_{n+1(z=1)} = \frac{\Delta t}{\Delta t_l}\widehat{\boldsymbol{P}}^s_{n+1} + \left[1 - \frac{\Delta t}{\Delta t_l}\right]\boldsymbol{P}^s_n. \tag{24}$$

Apparently, the domain switching process might take several incremental steps to be completed if Δt is much smaller than Δt_l. Based on the elaborations above, we obtain the following expression for the nucleation at time $t_s + z\Delta t$

$$\begin{aligned}\boldsymbol{P}^s_{n+1(z)} &= \frac{\Delta t}{\Delta t_l}\widehat{\boldsymbol{P}}^s_{n+1} + \left[\frac{[z-1]\Delta t}{\Delta t_l}\right]\widehat{\boldsymbol{P}}^s_{n+1} \\ &\quad + \left[1 - \frac{[z-1]\Delta t}{\Delta t_l} - \frac{\Delta t}{\Delta t_l}\right]\boldsymbol{P}^s_n \\ &= \frac{\Delta t}{\Delta t_l}[\widehat{\boldsymbol{P}}^s_{n+1} - \boldsymbol{P}^s_n] + \left[\frac{[z-1]\Delta t}{\Delta t_l}\right]\widehat{\boldsymbol{P}}^s_{n+1} \\ &\quad + \left[1 - \frac{[z-1]\Delta t}{\Delta t_l}\right]\boldsymbol{P}^s_n \\ &= \boldsymbol{P}^s_{n+1(z-1)} + \frac{\Delta t}{\Delta t_l}\left[\widehat{\boldsymbol{P}}^s_{n+1} - \boldsymbol{P}^s_n\right],\end{aligned} \tag{25}$$

whereby $\Delta t = \text{constant}$ has been assumed. Eq. (25) motivates to iterate this update until $z\Delta t \geqslant \Delta t_l$ so that finally $\boldsymbol{P}^s_{n+1} = \widehat{\boldsymbol{P}}^s_{n+1}$, i.e., switching has been completed.

4. Finite element setting

In this section we review the algorithmic setting which will enable us to run representative numerical simulations. In particular, the finite element method is used and applied within a three-dimensional context. The underlying equations for the piezoelectric finite element formulation are derived from the principle of virtual work as based on the piezoelectric constitutive laws and balance equations. In this work, however, we consider solely electrical loading—the fully coupled setting will be elaborated in a subsequent contribution. The boundary value problem is therefore given by the set of equations (2) wherein the electric displacement boils down to

$$\boldsymbol{D} = \boldsymbol{\epsilon} \cdot \boldsymbol{E} + \boldsymbol{P}^s, \tag{26}$$

compare Eq. (6). As a consequence, neither the elastic stiffness $\mathbf{C}$ nor the piezoelectric constant $\boldsymbol{d}$ but solely the dielectric permittivity $\boldsymbol{\epsilon}$ enter the incorporated constitutive equation (26). In view of experimental settings, the (essential) boundary conditions ϕ^p on $\partial\mathscr{B}_\phi$ might be covered by electrodes (prescribing the electric potential) while the (natural) boundary condition q^p on $\partial\mathscr{B}_D$ represent a prescribed charge.

With these definitions at hand, the corresponding weak form results in

$$G_\phi = -\int_{\mathscr{B}} \delta\boldsymbol{E} \cdot \boldsymbol{D}\,\mathrm{d}v - \int_{\partial\mathscr{B}_D} \delta\phi q\,\mathrm{d}a = G^{\text{int}}_\phi - G^{\text{ext}}_\phi = 0. \tag{27}$$

Following standard finite element techniques, the linearized incremental representation—for dead loading conditions—results on the element level in

$$\Delta G^e_\phi = \int_{\mathscr{B}^e} -\delta\boldsymbol{E} \cdot [\boldsymbol{\epsilon} \cdot \Delta\boldsymbol{E} + \Delta\boldsymbol{P}^s]\,\mathrm{d}v. \tag{28}$$

Adopting an iso-parametric interpolation renders the approximated electric potential ϕ, which constitutes the remaining degree of freedom, $\delta\phi$ and $\Delta\phi$ as well as $\boldsymbol{x}$ as

$$\begin{aligned}\phi^h &= \sum_{i=1}^{n_{el}} N_i\phi_i, \\ \delta\phi^h &= \sum_{i=1}^{n_{el}} N_i\delta\phi_i, \\ \Delta\phi^h &= \sum_{i=1}^{n_{el}} N_i\Delta\phi_i, \\ \boldsymbol{x}^h &= \sum_{i=1}^{n_{el}} N_i\boldsymbol{x}_i,\end{aligned} \tag{29}$$

wherein n_{el} denotes the number of nodes in a finite element and N_i characterize the shape functions. Consequently, the approximation of the electric field $\boldsymbol{E}$, $\delta\boldsymbol{E}$ and $\Delta\boldsymbol{E}$ read

$$\begin{aligned}\boldsymbol{E}^h &= -\sum_{i=1}^{n_{el}} \phi_i\nabla N_i, \\ \delta\boldsymbol{E}^h &= -\sum_{i=1}^{n_{el}} \delta\phi_i\nabla N_i, \\ \Delta\boldsymbol{E}^h &= -\sum_{i=1}^{n_{el}} \Delta\phi_i\nabla N_i.\end{aligned} \tag{30}$$

Based on these assumptions, G_ϕ allows representation on the element level as

$$G^e_\phi = \int_{\mathscr{B}^e} \sum_i^{n_{el}} \delta\phi_i[\nabla N_i \cdot \boldsymbol{D}]\,\mathrm{d}v - \int_{\partial\mathscr{B}^e_D} \sum_i^{n_{el}} \delta\phi_i[N_i q]\,\mathrm{d}a = 0. \tag{31}$$

Similarly, we obtain for Eq. (28)

$$\Delta G^e_\phi = \int_{\mathscr{B}^e} -\sum_{i,j}^{n_{el}} \delta\phi_i[\nabla N_i \cdot \boldsymbol{\epsilon} \cdot \nabla N_j]\Delta\phi_j\,\mathrm{d}v. \tag{32}$$

Please note that $\Delta\boldsymbol{P}^s$ is not incorporated into Eq. (32) since we do not apply standard implicit and monolithic iteration schemes in what follows but rather a staggered technique which turns out to perform very robust. A graphical representation of the implemented algorithm is summarized in the flowchart in Table 1. The spontaneous polarization field $\boldsymbol{P}^s$ itself, however, is included within Eq. (31) and therefore accounted for in a, say, residual manner. The non-linearity of the proposed formulation stems from the (time dependent) switching of the polarization vector.

Table 1
Flowchart of the applied finite element algorithm

```
loop over all time steps
  global load step
    loop over all elements
      loop over all integration points
      compute E^e, D^e and r^e_φ, K^e_φφ
    assemble r_φ, K_φφ
  update φ
  loop over elements
    loop over all integration points
    check switching criterion
  update P^se
  recompute φ with updated P^se
    loop over all elements
      loop over all integration points
      compute E^e, D^e and r^e_φ, K^e_φφ
    assemble r_φ, K_φφ
  update φ
determine actual (nucleated) state
```

Practically speaking, the bracket terms in Eqs. (31) and (32) render, after assembly with respect to the global finite element level, the residual vector $\mathbf{r}_\phi$ and the (incremental) tangent stiffness $\mathbf{K}_{\phi\phi}$. In order to save computation time, the incremental switching process within one time step is stopped as soon as one particular finite element has been identified to switch, compare Table 1. This assumption restricts the proposed formulation—nevertheless, consideration of small time steps yields realistic simulations, see Section 5.

5. Numerical examples

The computation of the material behavior is performed within the above highlighted three-dimensional finite element scheme. Some hundreds of crystallites are modeled so that each finite element represents one crystallite, see the graphical representation in Fig. 4. Moreover, we assume the polarization vector to be constant within one element, or rather crystallite, and choose a random orientation for the initial polarization vector. In particular, a parameterization with respect to three Euler angles (Θ, Φ, Ψ) is adopted so that the directions of initial polarization vectors allow representation as

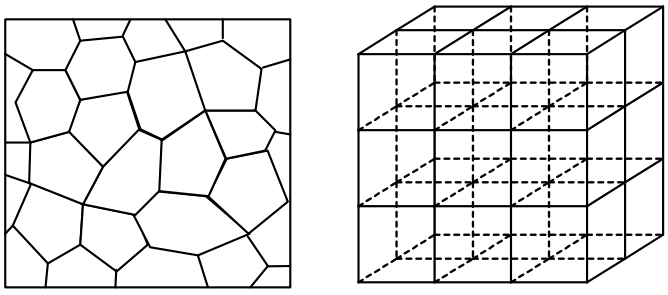

Fig. 4. Natural assembly of grains and corresponding finite element discretization.

$$\begin{aligned}\boldsymbol{P}^{\mathrm{s}}/P^{\mathrm{s}} = {} & [\mathrm{c}(\Theta)\mathrm{s}(\Phi)\mathrm{c}(\Psi) + \mathrm{c}(\Phi)\mathrm{s}(\Psi)]\boldsymbol{e}_1 \\ & - [\mathrm{c}(\Theta)\mathrm{s}(\Phi)\mathrm{s}(\Psi) - \mathrm{c}(\Phi)\mathrm{c}(\Psi)]\boldsymbol{e}_2 - [\mathrm{s}(\Theta)\mathrm{s}(\Phi)]\boldsymbol{e}_3,\end{aligned} \tag{33}$$

wherein the notations c(·) and s(·) abbreviate cos(·) and sin(·), respectively, and $\{\boldsymbol{e}_{1,2,3}\}$ denotes a Cartesian frame which is fixed in space.[1] The random generation of the Euler angles provides $\Theta, \Psi \in [0, 2\pi]$ and $\sin(\Phi - \frac{\pi}{2}) \in [-1, 1]$. The spontaneous polarization magnitude is assumed to be identical for all unit cells, namely $P^{\mathrm{s}} = P_0$ and the polarization vectors themselves are stored as internal variables at the integration point level. After an incremental load step has been applied, the crystallites are checked whether the switching criterion (14) is met, compare Table 1. The energy criterion is represented by the volume averaging with respect to one finite element as based on the integration point fields, e.g.,

$$\overline{\boldsymbol{E}}^{\mathrm{e}} = \frac{1}{\mathscr{V}^{\mathrm{e}}} \int_{\mathscr{V}^{\mathrm{e}}} \boldsymbol{E}^{\mathrm{e}} \, \mathrm{d}v. \tag{34}$$

According to this criterion, domain switching occurs if the energy change is larger than a certain critical level for one element at a time. The critical energy barrier is assumed to be identical for 90° and 180° switching within the subsequent simulations, compare Section 2. If switching occurs according to the mentioned criterion, new polarization vectors are incorporated into Eq. (31) which results in an updated electric potential. As previously mentioned, we assume only one domain to switch at each incremental load step (due to the computational efficiency). Even though this assumption is not realistic, the proposed formulation turns out to be acceptable when the number of finite elements is sufficiently large and the applied time steps are sufficiently small. Furthermore, intergranular effects stemming from different polarization directions of different grains are observed which, for instance, result in the development of inter-domain stresses under electrical or mechanical loading. The corresponding local electromechanical loading state might considerably vary between grains, so that domain switching for some lattice structures can occur even before the assumed global critical electromechanical field level (this global level will be denoted as the macroscopic coercive electric field in the progression of this contribution). As a result, non-linear response is observed even in a small electromechanical loading range. In order to take this effect into account, which becomes especially relevant in the domain switching range, the proposed formulation

[1] Please note that the local orthonormal frame $\{\boldsymbol{m}_{1,2,3}\}$, which defines the symmetry of each individual grain, is defined via

$$\begin{aligned}\boldsymbol{m}_2 &= \boldsymbol{P}^{\mathrm{s}}/P^{\mathrm{s}}, \\ \boldsymbol{m}_1 &= [\mathrm{c}(\Theta)\mathrm{c}(\Phi)\mathrm{c}(\Psi) - \mathrm{s}(\Phi)\mathrm{s}(\Psi)]\boldsymbol{e}_1 \\ &\quad - [\mathrm{c}(\Theta)\mathrm{c}(\Phi)\mathrm{s}(\Psi) + \mathrm{s}(\Phi)\mathrm{c}(\Psi)]\boldsymbol{e}_2 \\ &\quad + [\mathrm{s}(\Theta)\mathrm{c}(\Phi)]\boldsymbol{e}_3, \\ \boldsymbol{m}_3 &= \boldsymbol{m}_1 \times \boldsymbol{m}_2\end{aligned}$$

with $\boldsymbol{m} = \boldsymbol{m}_2$, compare Section 2.

incorporates an additional probability function for the domain switching. In what follows, we assume this function to be determined via the polynomial

$$P = \begin{cases} \left[\dfrac{\overline{\boldsymbol{E}}^{\mathrm{e}} \cdot \Delta \boldsymbol{P}^{\mathrm{se}}}{2E_0P_0}\right]^k & \text{for } E < E_0, \\ 1 & \text{for } E \geqslant E_0 \end{cases} \tag{35}$$

so that the applied switching criterion results in

$$\overline{\boldsymbol{E}}^{\mathrm{e}} \cdot \Delta \boldsymbol{P}^{\mathrm{se}} > 2E_0P_0P, \tag{36}$$

compare Eq. (14).[2] In this context, intergranular effects are phenomenologically taken into account and non-linear response might occur at loading levels which are below the usual critical loading. The additional material parameter $k > 0$ in Eq. (35) allows matching numerical results with respect to experimental data. For the subsequent simulation appropriate congruence is obtained for, e.g., $k = 5$.

For the subsequent finite element calculations we consider a specimen arranged in a $9 \times 9 \times 9$ block. The discretization is performed with $9 \times 9 \times 9$ linear eight node bricks (Q1)—their edges being parallel to the global Cartesian frame $\{\boldsymbol{e}_{1,2,3}\}$, see Fig. 5. Loading is applied in terms of a prescribed electric potential at the top—, $\phi^{\mathrm{p}}_{\mathrm{top}}$, and bottom surface, $\phi^{\mathrm{p}}_{\mathrm{bot}}$, which are assumed to lie in the $\boldsymbol{e}_1$–$\boldsymbol{e}_2$ plane. The electric potential is throughout zero at nodal points on the bottom surface while the electric potential on the top surface, which is uniform, is incrementally prescribed according to the particular time step. Charge free conditions are applied to the remaining surfaces. For the purpose of illustration, volume averaged electric displacements are plotted over the electric field

$$\begin{aligned} \mathsf{D} &= \boldsymbol{e}_3 \cdot \frac{1}{\mathscr{V}} \int_{\mathscr{V}} \boldsymbol{D}\, \mathrm{d}v, \\ \mathsf{E} &= \boldsymbol{e}_3 \cdot \frac{1}{\mathscr{V}} \int_{\mathscr{V}} \boldsymbol{E}\, \mathrm{d}v, \end{aligned} \tag{37}$$

both with respect to the loading direction $\boldsymbol{e}_3$.

5.1. Hysteresis loop for the rate-independent model

To set the stage, we discuss the rate-independent case in this section. The rate-independent model is conceptually included in the rate-dependent formulation highlighted in Section 3 by directly setting

$$\boldsymbol{P}^{\mathrm{s}}_{n+1} = \widehat{\boldsymbol{P}}^{\mathrm{s}}_{n+1} = \boldsymbol{P}^{\mathrm{s}}_{n} + \Delta \boldsymbol{P}^{\mathrm{s}}, \tag{38}$$

the additional index z becoming redundant since $\Delta t/\Delta t_1 \geqslant 1$; compare Eqs. (11) and (25). Longitudinal cyclic loading is applied in what follows. The starting point for the first cycle is at zero potential for the un-poled ceramic. We adopt the following material parameters: $\epsilon = 0.0666$ [μF/m] (cf. Eq. (8)), $P^{\mathrm{s}} = P_0 = 0.1938$ [C/m^2] (cf. Eqs. (11) and (14)), $E_0 = 0.4$ [MV/m] (cf. Eq. (14)) and the initial polarization direction is randomly generated (cf. Eq. (33)).

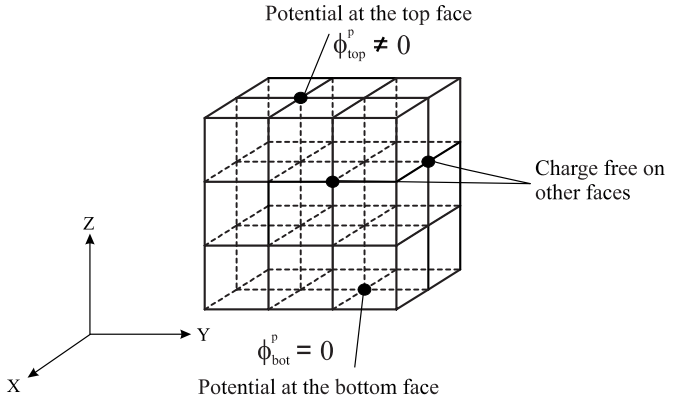

Fig. 5. Boundary conditions applied to the finite element discretization of the block-like specimen.

Fig. 6 shows the classical hysteresis loop by monitoring the electric displacement versus the electric field without considering a probability function ($k = 0$). It is clearly seen in Fig. 6 that the hysteresis curve possesses sharp corners near the macroscopic coercive electric field which is not observed in experiments. Fig. 7 shows the hysteresis loop based on the incorporation of a probability function with fourth order polynomial ($k = 4$). The smoothness of the curves near the critical electric field is clearly observed from Fig. 7. Fig. 8 displays the comparison of the simulation with experimental data given in Lu et al. [26]. The simulation is preformed with a fifth order probability function ($k = 5$) which nicely matches the experimental results.

5.2. Hysteresis loop for the rate-dependent model

Next, we discuss the rate-dependent case in this section whereby longitudinal cyclic loading is applied. The starting point for the first cycle is at zero potential for the un-poled ceramic. The simulations are performed for three different frequencies (0.01 Hz, 0.10 Hz, 1.00 Hz) and for different amplitudes of the electric field ($\widehat{\mathsf{E}} = 2.0$ MV/m, $\widehat{\mathsf{E}} = 1.5$ MV/m, $\widehat{\mathsf{E}} = 1.0$ MV/m). These particular values are chosen for comparison reasons of the numerical simulations with the experiments performed by Zhou et al. [38]. We adopt the following material parameters: $\epsilon = 0.02124$ [μF/m] (cf. Eq. (8)), $P^{\mathrm{s}} = P_0 = 0.4$ [C/m^2] (cf. Eqs. (11) and (14)), $E_0 = 1.0$ [MV/m] (cf. Eq. (14)), $C = 0.07$ (cf. Eq. (16)), the particular value being identified from experiments reported by Merz [29], and the initial polarization direction is randomly generated (cf. Eq. (33)).

Figs. 9–11 show the hysteresis curve for various loading amplitudes and frequencies. It is experimentally observed that the macroscopic coercive electric field depends on

[2] Apparently, solely one type of 90° switching and 180° switching might become relevant. The one being realized refers to the largest change in energy as represented by Eq. (36). However, even the polarization vector orientation which leads to the lowest possible energy level might violate the switching criterion. It is obvious that in this particular case no further switching is incorporated.

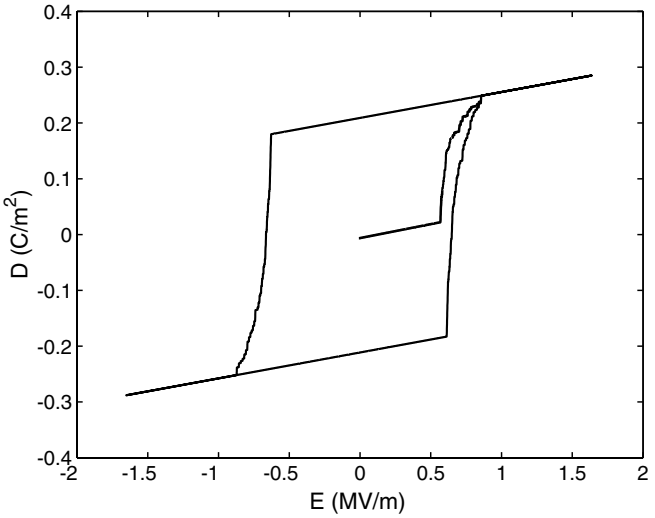

Fig. 6. Hysteresis curve without probability function ($k = 0$).

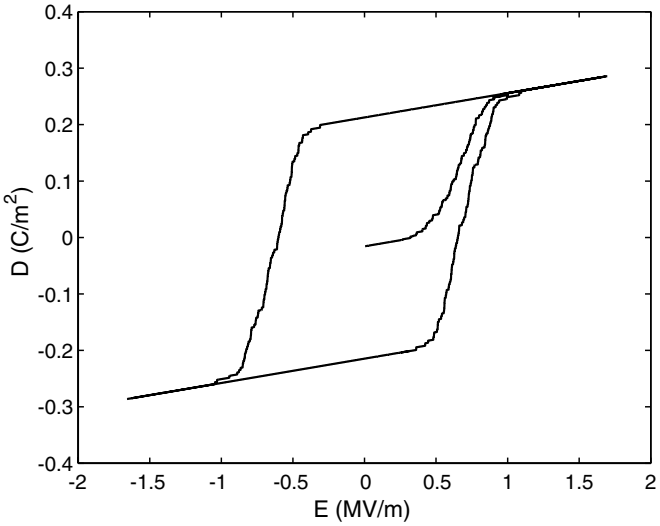

Fig. 7. Hysteresis curve with fourth order probability function ($k = 4$).

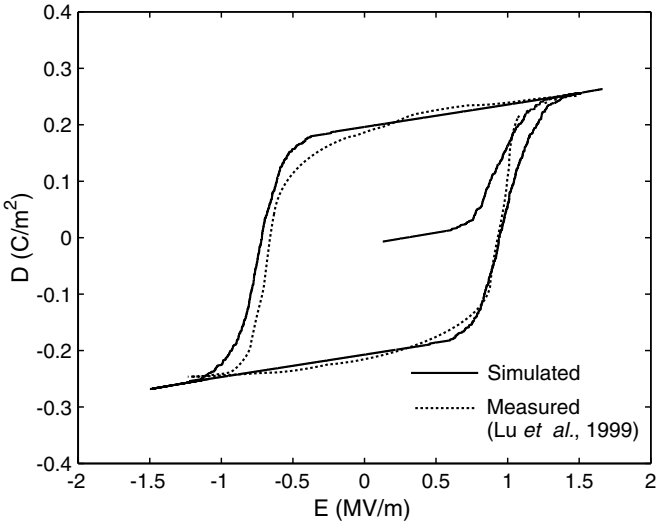

Fig. 8. Hysteresis curve with fifth order probability function ($k = 5$) and experimental data.

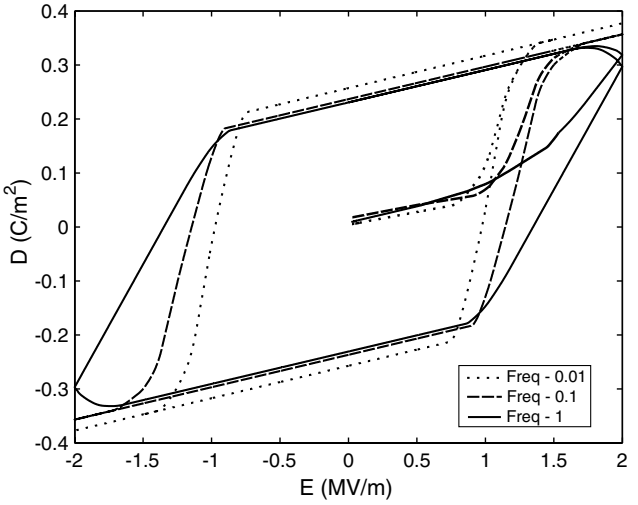

Fig. 9. Hysteresis curve without probability function ($k = 0$); $\hat{E} = 2.0$ [MV/m].

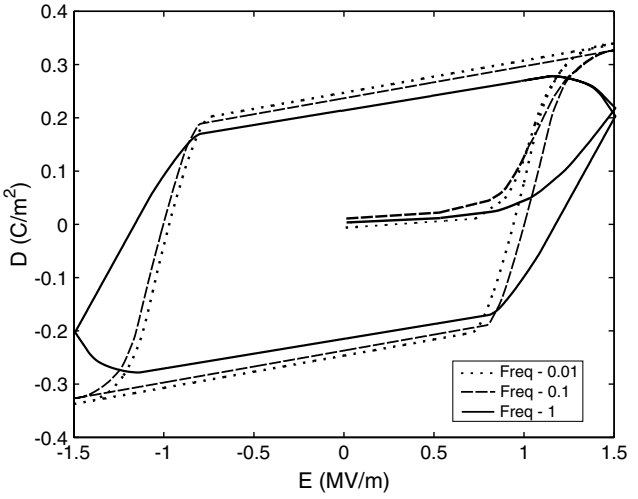

Fig. 10. Hysteresis curve without probability function ($k = 0$); $\hat{E} = 1.5$ [MV/m].

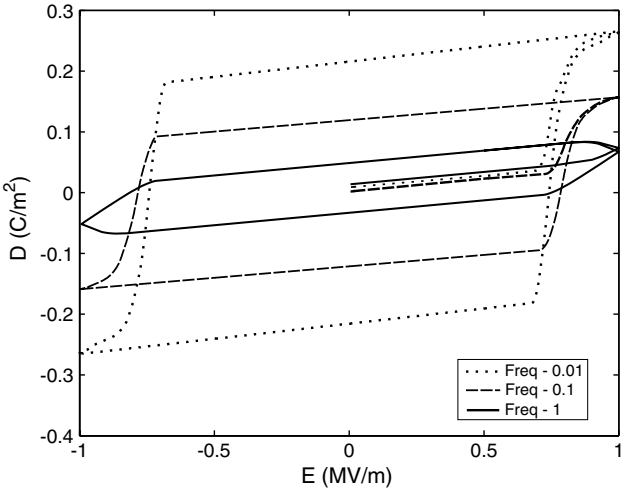

Fig. 11. Hysteresis curve without probability function ($k = 0$); $\hat{E} = 1.0$ [MV/m].

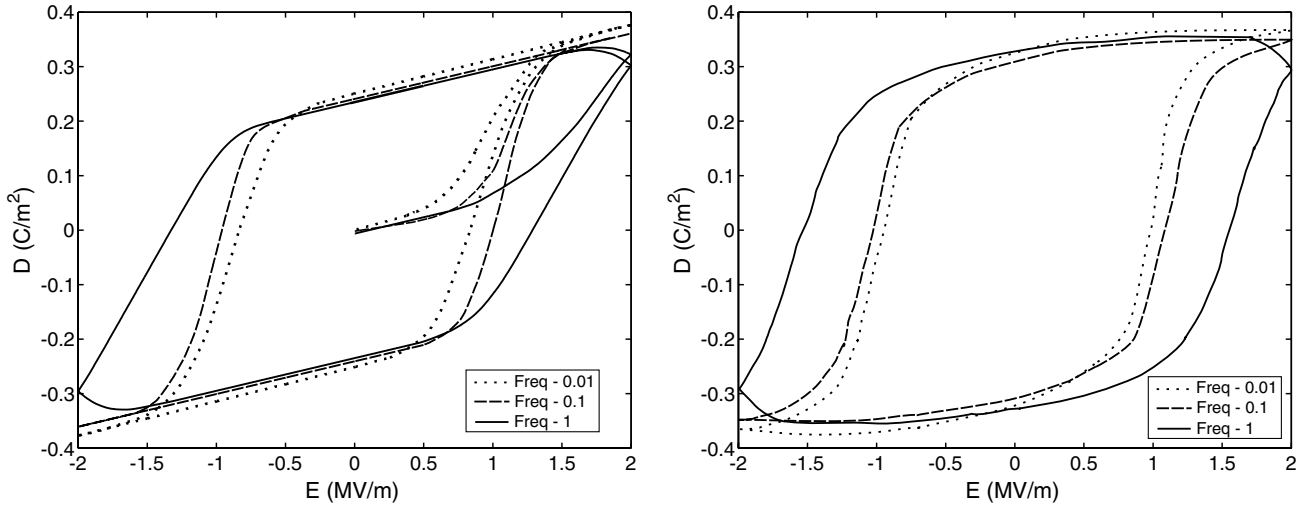

Fig. 12. Hysteresis curve with fifth order probability function ($k = 5$), (left) and experimental data—Zhou et al. [38], (right); $\widehat{E} = 2.0$ [MV/m].

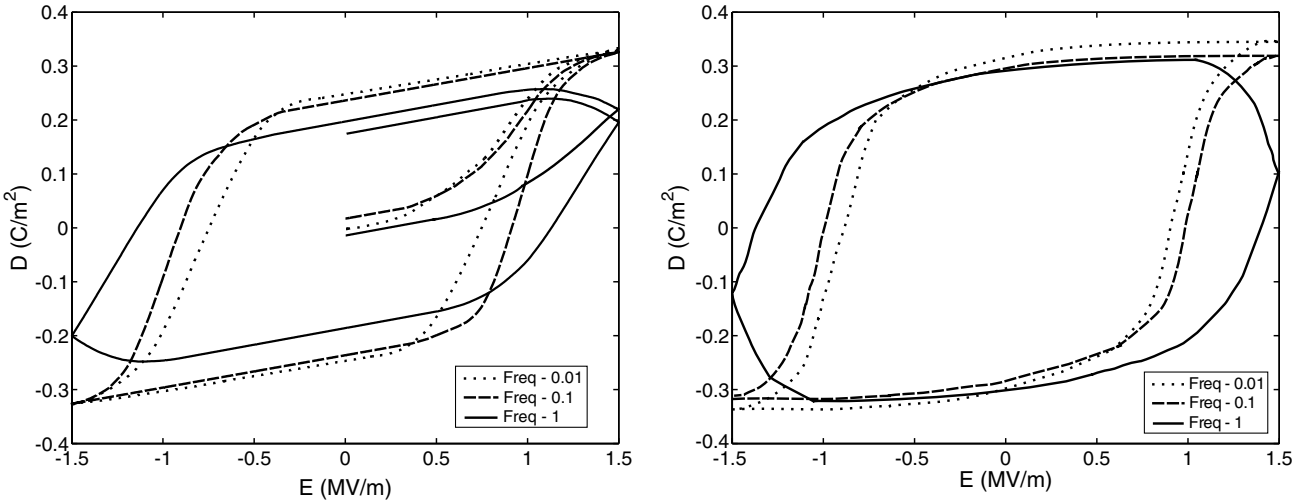

Fig. 13. Hysteresis curve with fifth order probability function ($k = 5$), (left) and experimental data—Zhou et al. [38], (right); $\widehat{E} = 1.5$ [MV/m].

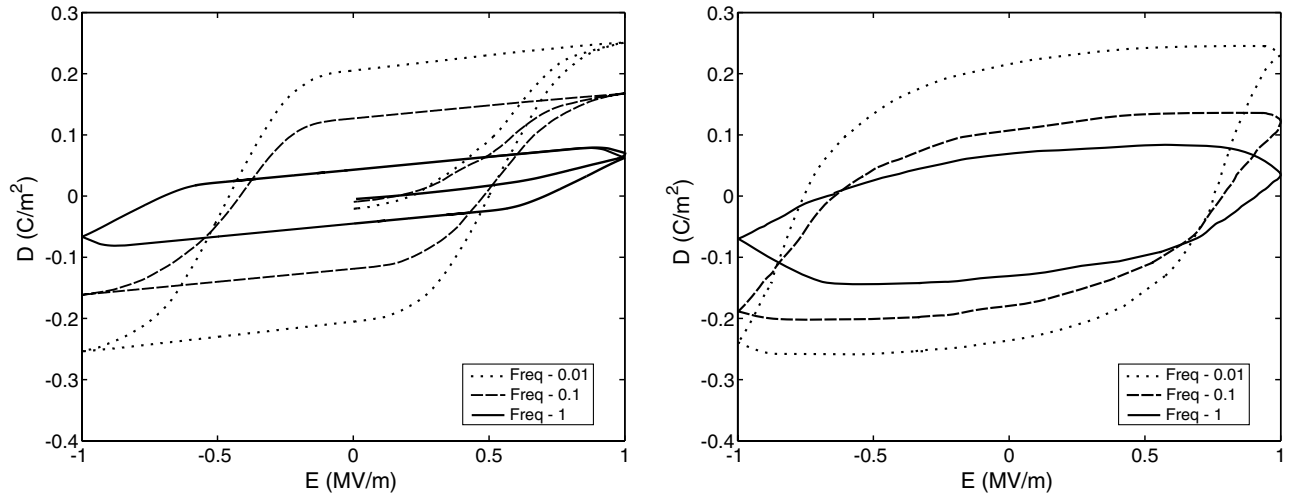

Fig. 14. Hysteresis curve with fifth order probability function ($k = 5$), (left) and experimental data—Zhou et al. [38], (right); $\widehat{E} = 1.0$ [MV/m].

the loading frequency which is monitored by the numerical results in Figs. 9–11. The macroscopic coercive electric field increases for higher loading frequency (0.01 Hz, 0.10 Hz, 1.00 Hz) irrespective of the loading amplitudes. We observe that the electric displacements increase for higher loading frequencies—even if the amplitude of the electric field decreases. The results monitored in Figs. 9 and 10 allow interpretation as the evolution of the electric displacements not being saturated for a loading frequency of 1.00 Hz compared to an almost quasi-static loading at 0.10 Hz or 0.01 Hz. Instead, the electric displacement increases for a decreasing electric field (for 1.00 Hz) until the electric field is smaller than the coercive electric field. Figs. 9 and 10 show that the remanent polarization (i.e., the electrical displacement at zero electric field) is not varying that much for the frequencies 0.01 Hz and 0.10 Hz. This effect stems from the fact that possible domain switchings are more or less completed after one simulation step. It can be observed in Fig. 11 that the remanent polarization is decreasing if the frequency of the cyclic loading is increased. This property stems from the influence of the loading frequency on the remanent polarization—especially when the amplitude of the applied electric field is in the range of the coercive field and the saturated polarization state has not been achieved.

Figs. 12–14 (left) show the simulated hysteresis curves for various amplitudes whereby intergranular effects are taken into account by means of the proposed probabilistic approach. The simulations are performed with a fifth order polynomial for the probability function ($k = 5$). One clearly observes that the computed curves are smooth near the macroscopic coercive field which is not the case in Figs. 9–11 for the simulations without introducing a probability for switching. Figs. 12–14 (right) show corresponding experimentally measured hysteresis curves for various loading amplitudes taken from Zhou et al. [38]. It is obvious that the computations including the probabilistic approach show a better match with the experimental results compared to those simulations which did not incorporate the probability function. Moreover, the curves in Figs. 12–14 (left) also reveal similar observation as those in Figs. 9–11: with increasing loading frequency the macroscopic coercive field is also increasing and the remanent polarization increases at lower loading amplitudes. As a general rule, the electric displacement increases at higher loading frequencies until the macroscopic coercive field is reached.

6. Summary

A three-dimensional micro-mechanically motivated model based on the free energy, a switching criterion, a probabilistic approach and linear kinetics for domain switching of piezoelectric materials has been presented and implemented into a non-linear finite element program. Simulations are discussed for a longitudinal high cyclic electric loading at various loading frequencies and amplitudes. Non-homogeneities stem from the polarization vectors which are initially generated by random. Intergranular effects between different domains have been phenomenologically accounted for by means of a probability function. The simulated results are in good qualitative agreement with experimental data. A linear kinetics theory successfully described fundamental characteristics of piezoelectric materials at different loading rates and amplitudes such as the change of the macroscopic coercive field and of the remanent polarization. Elaborations on the derivation of rate-dependent effects under coupled electromechanical loadings constitute future research.

Acknowledgements

The authors thank the 'Deutsche Forschungsgemeinschaft (DFG)' for financial support of this work within the 'Graduiertenkolleg 814, Ingenieurmaterialien auf verschiedenen Skalen: Experiment, Modellierung und Simulation'.

References

[1] R. Abeyaratne, S.J. Kim, J.K. Knowles, Int. J. Solids Struct. 31 (1994) 2229–2249.
[2] G. Arlt, Ferroelectrics 189 (1996) 103–119.
[3] G. Arlt, Ferroelectrics 189 (1996) 91–101.
[4] G. Arlt, Integr. Ferroelectr. 16 (1997) 229–236.
[5] H. Cao, A.G. Evans, J. Am. Ceram. Soc. 76 (1993) 890–896.
[6] P.J. Chen, P.S. Peercy, Acta Mech. 31 (1979) 231–241.
[7] X. Chen, D.N. Fang, K.C. Hwang, Acta Mater. 45 (1997) 3181–3189.
[8] B. Delibas, A. Arockiarajan, W. Seemann, Int. J. Solids Struct. (2005), available online.
[9] M. Elhadrouz, T.B. Zineb, E. Patoor, Comput. Mater. Sci. 32 (2005) 355–359.
[10] A.C. Eringen, Mechanics of Continua, Krieger Publishing Company, Florida, 1989.
[11] Y. Fotinich, G.P. Carman, J. Appl. Phys. 88 (2000) 6715–6725.
[12] Y. Fotinich, G.P. Carman, Ferroelectrics 274 (2002) 101–119.
[13] W. Greiner, Classical Electrodynamics, Springer, New York, 1998.
[14] J.E. Huber, N.A. Fleck, Eur. J. Mech. A/Solids 23 (2004) 203–217.
[15] S.C. Hwang, J.E. Huber, R.M. McMeeking, N.A. Fleck, J. Appl. Phys. 84 (1998) 1530–1540.
[16] S.C. Hwang, C.S. Lynch, R.M. McMeeking, Acta Metal. Mater. 5 (1995) 2073–2084.
[17] S.C. Hwang, R.M. McMeeking, Ferroelectrics 211 (1998) 177–194.
[18] S.C. Hwang, R.M. McMeeking, Int. J. Solids Struct. 36 (1999) 1541–1556.
[19] S.C. Hwang, R. Waser, Acta Mater. 48 (2000) 3271–3282.
[20] B. Jaffe, W.R. Cook, H. Jaffe, Piezoelectric Ceramics, Academic Press, London, New York, 1971.
[21] Q. Jiang, J. Elast. 34 (1994) 1–21.
[22] M. Kamlah, U. Böhle, Int. J. Solids Struct. 38 (2001) 605–633.
[23] M. Kamlah, C. Tsakmakis, Int. J. Solids Struct. 36 (1999) 666–695.
[24] S.J. Kim, Q. Jiang, Int. J. Solids Struct. 39 (2002) 1015–1030.
[25] C.M. Landis, J. Mech. Phys. Solids 50 (2002) 127–152.
[26] W. Lu, D.-N. Fang, C.Q. Li, K.C. Hwang, Acta Mater. 47 (1999) 2913–2926.
[27] C.S. Lynch, Acta Mater. 44 (1996) 4137–4148.
[28] R.M. McMeeking, S.C. Hwang, Ferroelectrics 200 (1997) 151–173.
[29] W.J. Merz, Phys. Rev. 95 (3) (1954) 690–698.

[30] J.F. Nye, Physical Properties of Crystals—Their Representation by Tensors and Matrices, Oxford Science Publications, Oxford, 1985.
[31] H. Romanowski, J. Schröder, in: Y. Wang, K. Hutter (Eds.), Trends in Applications of Mathematics to Mechanics, Shaker Verlag, Aachen, 2005, pp. 419–428.
[32] J. Schröder, D. Gross, Arch. Appl. Mech. 73 (2004) 533–552.
[33] J. Schröder, H. Romanowski, Arch. Appl. Mech., in press.
[34] W. Seemann, A. Arockiarajan, B. Delibas, Micromechanical simulation of piezoelectric materials using probability functions, in: Proc. SPIE, vol. 5387, 2004, pp. 57–64.
[35] P.P. Silvester, R.L. Ferrari, Finite Elements for Electrical Engineers, Cambridge University Press, Cambridge, 1996.
[36] R.C. Smith, Z. Ounaies, R. Wieman. A model for rate dependent hysteresis in piezoceramic materials operating in low frequencies. Technical Report 2001-26, NASA/CR-2001-211062, ICASE Report, Hampton, 2001.
[37] X.D. Zhang, C.A. Rogers, Int. J. Eng. Sci. 26 (1993) 1279–1306.
[38] D. Zhou, M. Kamlah, D. Munz, Rate dependence of soft PZT ceramics under electric field loading, in: Proc. SPIE, vol. 4333, 2001, pp. 64–70.